Laboratory Experiments on Arc Deflection and Instability

Stewart Zweben and Max Karasik
Princeton Plasma Physics Laboratory
P.O. Box 451, Princeton, NJ 08543

1. Introduction

This article describes experiments on arc deflection instability and carried out during the past few years at the Princeton University Plasma Physics Laboratory (PPPL). Our approach has been that of plasma physicists interested in arcs, but we believe these results may be useful to engineers who are responsible for controlling arc behavior in large electric steel furnaces.

Arcs are a type of "plasma," that is, a gas which is hot enough for some of the electrons to break free from the atoms (ionize) and conduct electricity. Arc temperatures are typically 10,000 ºC, which makes their electrical resistivity about 1,000 times higher than steel. This high resistance is desirable for the EAF application where the arc acts like a heating element in the EAF circuit. However, arcs (and most plasmas) are sensitive to deflection by magnetic fields and are generally unstable.

The behavior of arcs has been studied for many years [1-3], but the physical causes of arc deflection and instability in industrial-scale electric arc furnaces (EAFs) are not yet well understood. This is partly due to the obvious difficulties of making arc measurements inside an operating furnace, and partly due to the intrinsic complexity of arc behavior itself.

Our laboratory does plasma physics research with the long-term goal of practical fusion energy production. Fusion "furnaces" such as the Tokamak Fusion Test Reactor (TFTR) at PPPL [4] have plasma currents of 3 MA, diameters of 25', and heating powers of 40 MW, which produces a plasma temperature of up to 400,000,000 ºC. The horizontal and vertical location (i.e., deflection) of these plasmas is routinely controlled to well within 1 cm, and the large-scale plasma instabilities are successfully controlled during normal operation. Thus we had reasons to believe that arc deflection and instability can be controlled, although not in exactly the same way as in fusion plasmas.

The work described below was part of a Ph.D. thesis project to understand the physics of arc deflection and instability in laboratory-scale furnaces [5].

We have not had an opportunity to do systematic measurements or experiments on an industrial-scale furnace.

2. The PPPL Arc Furnace

A photo of the small PPPL arc furnace is shown in Fig. 1. It has a vertically movable graphite cathode of typically 3/8" diameter, and an iron or steel anode of 6" diameter. For unobstructed viewing access there is no slag and no shell, so arcs of $L \leq 10$ cm in length could be observed and photographed. The arc current was $I \leq 250$ amps with a DC power level ≤ 30 kW, so it is similar to a well-regulated DC arc welder. The arc was struck by touching the cathode to the anode and drawing the arc upward. It was run in air with ventilation but without water cooling, so the duration of each run was limited to 10-15 minutes to avoid overheating the enclosure.

Electromagnetic coils were placed on the sides and below the furnace to study the effects of magnetic fields on the arc deflection and instability. A spatially uniform horizontal magnetic field of $B \leq 10$ Gauss was created at the arc with a frequency from DC to 10 kHz, as measured directly using Hall and magnetic probes when the arc current was off. A gated, intensified CCD camera was used to photograph the arc light emission at a standard TV framing rate, but with a 10 μsec exposure per frame time to "freeze" the arc motion. The arc could also be viewed by eye through dark welding glass. Electrical measurements were made of the arc voltage and current from DC up to 2 kHz, and the arc location in the horizontal direction was measured with an array of fast photodiodes.

Parameters of the PPPL arc are compared with those of an industrial-scale EAF furnace in Table 1. Clearly some parameters are different, such as the ratio of the plasma pressure to the magnetic field pressure β and the Mach number of the arc jet flow, so caution should be used in applying these results to large furnaces, as discussed in Sec. 6.

3. Arc Deflection

It is known that undesirable arc deflection in EAFs or arc welders can be due to the stray magnetic fields created by the electrical buswork leading to arc [6-8]. In general, the arc is deflected by the $F_x = I_z \times B_y$ force due to the interaction of the arc current I_z and the magnetic field B_y perpendicular to the arc, where the force F_x is perpendicular to both I_z and B_y.

Typically the arc current I_z is vertical and the magnetic field caused by the external buswork is horizontal, so the $I_z \times B_y$ force tends to deflect the arc away from the furnace power supply, as illustrated schematically in Fig. 2. However, this effect can easily be modified in EAFs by the iron shell and unmelted scrap, which can shield magnetic fields from the arc itself, and by other factors such as the foamy slag or electrode geometry. In industrial furnaces the arc deflection angle is difficult to measure directly, and its relationship with the externally generated magnetic fields is not easy to evaluate.

In the PPPL arc deflection experiment, as described in detail in Ref. [9], we applied a uniform horizontal transverse field B_y to a stable vertical arc with a current I_z, and always saw a clear arc deflection in the expected $F_x = I_z \times B_y$ direction as illustrated in the CCD images shown at the top of Fig. 3. The arc maintains this steady deflected position as long as a steady transverse B_y field is applied. The parameters for Fig. 3 were B = 2 Gauss and I = 150 A, corresponding to a force on the arc of $F_x \approx 3 \times 10^{-2}$ N/m, or about 2×10^{-3} kg of force for an arc of length L ≈ 0.07m.

The simplest theoretical analysis of such arc deflection assumes the arc behaves like a thin wire with current I_z and linear mass density m (kg/m), acted on by the uniform transverse force $I_z \times B_y$ (N/m). The boundary conditions for this experiment are that the arc is fixed at the cathode and freely movable at the anode. A crucial element of this analysis is the arc jet speed v_z (m/s), which is assumed here to be a constant along the axial direction z of the arc (see below). With these assumptions, the deflected shape of the arc in the $I_z \times B_y$ or x direction is a parabola [9,10]:

$$x = [IB/(2mv_z^2)]\, z^2 = D\, z^2 \qquad [1]$$

In this equation the arc deflection coefficient $D = [IB/(2mv^2)]$ can be interpreted as the ratio of the transverse driving force per unit length $I_z \times B_y$ to the arc jet kinetic energy per unit length $mv_z^2/2$. Thus the transverse arc deflection "x" at a given distance from the cathode "z" increases linearly with I_z and B_y. Good fits of the observed arc shape to this parabolic model are obtained in the experiment, as shown at the bottom of Fig. 3.

The arc in this analysis acts like the jet from a water hose being blown in the wind — the deflection depends on the force of the wind, but also on the mass density and speed of the water jet. Thus the magnitude of the arc deflection can not be determined from I_z and B_y alone, but also requires a knowledge of both m and v_z. These parameters are difficult to measure directly in our small furnace (and even more difficult to measure in an industrial furnace).

A theory for determining the arc jet velocity was developed in the classic work of Maecker [11], and has been at least qualitatively verified in some controlled experiments [1-3]. The arc jet velocity is caused by a narrow constriction of the arc near the graphite cathode (the cathode "spot"), which is small due to the very high temperature required for the cathode to emit electrons. This arc constriction at the cathode spot increases the local self-magnetic field, which causes a radially inward magnetic pressure on the arc. The high collisionality of the arc causes the pressure to be transferred into the axial direction, which causes the plasma jet velocity directed down the length of the arc. This type of magnetic "pinch" is familiar in plasma fusion research, and is somewhat similar to the jet of water created by squeezing a plastic container with a narrow spout.

The maximum arc jet velocity near the cathode was derived by Maecker as [3,11]:

$$v_{z,max} \approx I\,(\mu_o/[2\pi^2\rho r_c^2])^{1/2} \qquad [2]$$

where r_c is the radius of the constricted arc at the cathode and ρ is the mass density of the arc per unit volume. This maximum velocity can be estimated using a typical arc current density of 3×10^7 A/m^2 [1,2], i.e. $r_c \approx 0.1$ cm at I = 150 A, and an assumed arc density corresponding to atmospheric pressure air at 10,000 ^{o}C, i.e. $\rho \approx 1.7 \times 10^{-2}$ kg/m^3. The velocity from Eq. 2 is then $v_{z,max} \approx$ 300 m/sec. Note that this is the peak jet speed at the cathode spot, not the average jet speed downstream, which can be slower due to mixing with air.

In our experiment the arc jet velocity was measured indirectly (i.e. without using Eq. [2]) by forcing the arc to oscillate transversely using an AC excitation of the external magnetic field coils shown in Fig. 1. The arc jet velocity can be then be inferred by measuring the wavelength of the resulting deflection pattern, similar to the way in which the velocity of a water jet can be measured by oscillating the position of the hose at a known frequency.

Some examples of the arc shapes in these AC deflection experiments are shown in Fig. 4 for external magnetic field strengths in the range $B_y \approx 3$ Gauss and driving frequencies in the range ≈500-1000 Hz. The arc was seen to wriggle in the plane perpendicular to the applied $B_y(t)$ in a very regular and repeating pattern. The amplitude of the AC arc deflection increases with the magnitude of the applied B_y, and the wavelength of the deflection decreases as the frequency and arc current increase. Note that the arc speed is still predominantly in the z-direction, but now the x-deflection at a given z-position oscillates in time due to the externally applied $B_y(t)$.

Digitized images of the arc shapes such as shown in Fig. 4 were interpreted using a generalized form of the arc deflection model of Eq. 1 in which the spatially uniform magnetic field causing the $I_z \times B_y$ deflection is assumed to oscillate at a frequency $f = 2\pi\omega$. The solution for the arc shape is then a growing sinusoid [9]:

$$x(z,t) = (IB/m\omega^2)\,[\cos(\omega t - \omega z/v) - \cos(\omega t) - (z\omega/v)\sin(\omega t - \omega z/v)] \qquad [3]$$

This solution reduces to Eq. [1] for $\omega z/v_z << 1$, i.e. the arc shape is only parabolic when the driving frequency is much less than the transit time of the arc jet from the cathode to the anode.

Fig. 5 shows examples of how the experimental data like that in Fig. 4 was fit to the theoretical model of Eq. 3. Such fits uniquely determine the two parameters m and v_z for a given I and B(ω). The results for our standard I = 150 A arc were $m = 5\pm1 \times 10^{-6}$ kg/m and $v_z = 23\pm2$ m/sec. This experimentally inferred linear mass corresponds to an arc temperature of about 7,000 °C for the visually observed arc column radius of ≈0.7 cm, which is reasonably close to the temperature measured for this type of arc [2,3,12]. This inferred jet velocity only about 1/10th of that predicted from the theory of Eq. 2, but is not unreasonable since Eq. 2 refers to the maximum jet speed near the cathode spot, and the measurement reflects the average speed along the whole arc column.

As a further check of this model, we show in Fig. 6 (left) the dimensionless form of the transverse deflection in Eq. 3, namely $M = [(IB/\omega)/mv_z]$, as a function of the magnitude of the applied magnetic field. This parameter M corresponds to the ratio of the transverse momentum imparted by the $I_z \times B_y$ force in a time (1/ω) to the axial momentum of the jet. The linearity of this relationship confirms that the observed AC deflection scales linearly with the applied field, i.e., the product mv_z inferred from these fits to Eq. 3 is independent of the applied field, as expected. On the right of Fig. 6 is shown the inferred jet velocity v_z for varying applied frequencies, which is constant, as expected, since the axial jet speed is determined at the cathode. For this value of jet velocity and a typical electrode separation, the low frequency parabolic solution is obtained for $\omega < 575$ sec^{-1}, i.e., below a frequency of 90 Hz, which is also consistent with the experimental observations.

In summary, the two experimental parameters m and v_z needed in the DC arc deflection model of Eq. 1 were indirectly determined by applying an externally oscillating magnetic field to the arc, and then fitting the resulting arc shapes to the AC arc deflection model of Eq. 3. Using these parameters, we can explain the magnitude and shape of the DC arc deflection for a given externally applied DC magnetic field.

These results imply that the DC deflection of an industrial-scale arc due to a known externally generated magnetic field can not be predicted without an independent knowledge of the effective arc mass density and jet velocity, which are difficult to measure directly. Possible applications of this result to industrial-scale furnaces are discussed in Sec. 5.

4. Arc Instability

Arc instability refers to any rapidly fluctuating arc shape which occurs spontaneously, independent of any externally driven arc deflection. It is well known that both DC and AC industrial-scale arc furnaces are highly unstable even during their "flat bath" state after the metal scrap is melted. The arc instability generates the very loud broadband acoustic noise around the furnace, with frequencies below 50 Hz to above 1,000 Hz [13]. There have been many attempts to characterize and understand this instability [14-19]. However, the undesirable power line "flicker" caused by arc instability is generally controlled using external reactances, rather than by directly stabilizing the arc itself.

The small PPPL arc furnace was also strongly unstable in some operation regimes, so a separate set of experiments was done to identify the cause of this instability. For these experiments the arc experiment was the same as in Sec. 3, but there was no externally applied magnetic field. A detailed description of these results can be found Ref. 20. As with the deflection experiments described above, caution must be used in applying our results to industrial-scale furnaces (see Sec. 5).

A typical case of arc instability is illustrated in Fig. 7. This arc was initially stable, but after about 1 minute of burning the arc began to "whistle" audibly, and formed a conical shape as viewed by eye. In this case the instantaneous shape of the unstable arc (as viewed with the 10 μsec exposure-time camera) was a 3-dimensional helix nearly fixed at the cathode and rotating in a few-cm diameter circle at the anode. The fundamental frequency of the arc motion was measured by a linear array of fast photodiodes to be ≈600 Hz, with a typical waveform as shown in Fig. 8. Also shown are waveforms of the measured arc current and voltage which also oscillated at this frequency.

The onset, amplitude, shape, and frequency of this arc instability varied considerably depending on the arc current, electrode separation and cathode geometry in this experiment [5,20]. For example: (a) for the normal 3/8" diameter cathode, the instability was never observed below I = 100 A, and

almost always occurred at I = 250 A, (b) its fundamental frequency was as low as ≈100 Hz near I = 100 A and as high as 800 kHz near I = 250 A, but had a considerable variation at each current, and (c) the arc instability sometimes became turbulent, with a broadband frequency spectrum extending from 1 Hz to 10 kHz, particularly when its amplitude was large.

However, the strongest factor which determined whether the arc was unstable or stable was the cathode geometry. The influence of the cathode geometry on arc instability has been observed previously [1,14,15], but apparently without a quantitative model relating it to the arc shape, which is discussed below.

The clearest example of this cathode geometry effect is illustrated in Fig. 9, which shows the arc shape for five different times during a single run with a "necked" graphite cathode of varying diameter. This I = 250 A arc was normally unstable for our standard 3/8" diameter graphite cathode, but whenever the cathode burned down to the smaller-diameter "necked" regions, the arc suddenly became stable. In fact, for cylindrical cathode shapes the I = 250 A arc was only unstable over a certain range of cathode areas from 20-30 mm^2, as shown in Fig. 10. For cathodes below and above this area the I = 250 A arc was stable for all arc lengths.

One other example is useful to motivate our model for arc instability. When the graphite cathode was made into a "paddle" shape 25 mm wide by 4 mm thick, as shown in Fig. 11, the wriggling arc motion was localized in the plane of the paddle, rather than in a cone as for the cylindrical cathode in Fig. 7. Thus both the onset of this instability and also its unstable shape depended critically on the cathode geometry, and only weakly on the arc current or arc length.

This dependence on cathode geometry suggest that this particular instability is caused by an unstable motion of the cathode attachment "spot," rather than by a magnetically-driven kinking of the arc itself. In our model, the observed shape of the arc motion is attributed to a rapid movement of the arc attachment point at the cathode, which, when combined with the arc jet velocity directed axially away from this spot, makes the observed wriggling pattern which oscillates in time and space. This is somewhat analogous to the wavy pattern formed in a jet from a water hose when its nozzle is wiggled.

A mathematical model for this type of arc instability was made by assuming that the arc had a constant axial (z-directed) velocity "v_z," and that the arc spot at the cathode was gyrating in a small circle in the x-y plane with a radius "a" and a frequency $f = 2\pi\omega$. The shape of the arc motion is then

a helix with a diameter which grows linearly with z, e.g., the shape in the (x-z) plane is [16]:

$$x(z,t) = a\,[\cos(\omega t - \omega z/v_z) - (z\omega/v_z)\sin(\omega t - \omega z/v_z)] \qquad [4]$$

Note that there is no force on the arc in this model, so the arc mass density does not enter into this solution - the arc plasma just moves transversely with a velocity of $v_x \leq \omega a << v_z$ after it leaves the cathode spot. This solution looks similar to that for the driven arc motion in Eq. 3, but actually represents a different physical situation.

Mathematical fits between Eq. 4 and the digitized shapes of various unstable arcs in this experiment are shown in Fig. 12. Good fits between this model and the data can be obtained using two adjustable parameters: the arc spot motion radius "a," and the arc jet velocity v_z. The arc jet velocities inferred from these fits agree to within ≈20% of those inferred from the driven arc motion, as expected.

The inferred values of the cathode spot motion parameter "a" for a database of unstable arcs is shown in Fig. 13, along with a few direct measurements of the visible cathode spot motion made using a magnifying lens. Both the inferred and measured cathode spot motion radii are $a \approx 0.15 \pm 0.1$ cm, which is comparable in size to the cathode spot itself, making this motion difficult to observe directly. The maximum transverse component of the arc velocity is thus $v_y \approx 2\pi(600\text{ Hz})(0.15\text{ cm}) \approx 4$ m/sec, which causes a transverse displacement of ≈0.8 cm at a distance of 4 cm from the cathode, as in the data at the bottom of Fig. 13. The resulting cone-shaped arc envelope is visible by eye during the arc instability.

Obviously, the next question is: what causes this unstable motion of the cathode spot? A necessary condition for cathode spot motion is that the surface temperature of the cathode must be sufficiently high for thermionic emission to sustain the arc current, i.e. roughly ≥3,500 ºC. This can explain why the arc is unstable for only a narrow range of cathode radii (Fig. 10): for larger radii the cathode bulk cools the surface surrounding the cathode spot below this temperature, and so the arc can not move, while for smaller radii the cathode size is comparable to the cathode spot size, so there is not enough room to move. Within this unstable range we believe that there is some mechanism(s) causing the cathode spot to rotate in a small circle, causing the helical arc pattern in the arc jet downstream.

However, we have not quantitatively understood the physical cause of the cathode spot motion in this experiment. The mechanisms which we have evaluated [5,20], some of which have been considered in previous studies, are:

a) resistive heating inside the graphite cathode due the arc current increases its temperature and electrical resistivity, and so causes the internal current path to move to a cooler region of the cathode. However, the timescale for bulk heating of a cathode volume comparable to the cathode spot radius would be ≈1 sec, so this could not explain the observed instability at ≈ 500 Hz,

b) surface heating of the cathode due to the ion flow or radiation from the arc could also increase its resistance locally and cause the cathode spot to move to a cooler region. However, the timescale for a significant local resistance change due to this surface heating is similar to the estimate in (a), so this could not explain the observed instability at ≈500 Hz,

c) cathode erosion will cause the local shape of the cathode surface to change, which could cause the arc to move. Since the arc tends to orient itself perpendicular to the cathode surface, this effect might move the arc away from any local hole caused by cathode erosion. However, the measured erosion rate of ≈0.06 mm/sec is too small to make a significant cathode spot motion on the timescale of the arc instability,

d) constriction of the arc current at the cathode spot can cause a magnetic interaction between the cathode current and the arc current, resulting in an unstable equilibrium. If a slight angle is created between these currents, their magnetic interaction tends to increase this angle, until the arc reaches a the edge of the cathode tip where this angle is a maximum. The timescale for such movement could be rapid enough to cause the instability, since the resistive diffusion time of current in the arc or cathode is very small ($<10^{-5}$ sec). However, we do not understand what could cause the arc to continue to move once it reaches the edge of the cathode,

e) vaporization of the graphite at the cathode spot could cause a local cooling of the arc itself, since the neutral gas is at most 4,000 ^{o}C and the arc plasma is about 10,000 ^{o}C. This cooling would cause the arc's resistivity to increase, and the arc current distribution would tend to move elsewhere. The timescale for this movement would be limited by the time to heat an adjacent area on the cathode surface to 4,000 ^{o}C, which we estimate to be $\approx 10^{-3}$ sec for the energy flux of $\approx 10^{8}$ W/m^{2} estimated at the cathode surface. This mechanism could produce a cathode spot velocity of up to 100 m/sec, which is more than enough to explain the inferred spot velocity of 4 m/sec.

In summary, the arc instability in our experiment seems to be caused by a small transverse motion of the arc attachment spot at the cathode surface, and not by a magnetic or aerodynamic instability of the arc itself. This model explains the observed conical shape of the unstable arc, and also the

sensitivity of its onset and shape to the cathode size and shape. However, further experiments and analysis is needed before we can understand the mechanism of the arc motion at the cathode which presumably causes this instability (see Sec. 6).

5. Potential Application to Industrial Furnaces

This section describes some potential applications of these results to industrial-scale EAFs. Here we will *assume* that the mechanisms of arc deflection and instability are similar to those in our small experiment. This is a debatable assumption, considering the differences in physical parameters illustrated in Table 1. Further research needed to understand the physics of high current arcs is described in Sec. 6.

a) Arc deflection in an large DC furnace:

First we will estimate the arc deflection angle for a 100 MW DC furnace based on the simplified models of Sec. 3. For this we need to estimate the transverse magnetic field B, the arc jet speed $v_{z,}$ and linear mass density m used in the arc deflection coefficient $D = [IB/(2mv_z^2)]$ in Eq. 1.

For a DC furnace with current of I = 100 kA and a shell radius of R = 5 m, the horizontal magnetic field at the arc due to the buswork shown Fig. 2 would be approximately $B_y = \mu_o I/2\pi R \approx 50$ Gauss, assuming no shielding from iron in the shell or unmelted scrap. The maximum arc jet velocity can be estimated from Eq. 2. For a typical arc current density at the cathode of 3×10^7 A/m^2, the arc radius at the cathode would be $r_c \approx 3$ cm. For an arc density of $\rho \approx 1.7 \times 10^{-2}$ kg/m^3 corresponding to atmospheric pressure at 10,000 ^{o}C, the maximum arc jet velocity would be (from Eq. 2) $v_{z,max} \approx$ 7,000 m/sec. This is probably too high, since our measured arc jet speed was only ≈1/10 of the estimate based on Eq. 2, and since this is about five times the sound speed at this temperature. Thus we will assume an average jet speed of 1000 m/sec and an arc of average diameter 10 cm, which is similar to that measured previously in high current arcs [1,2].

Thus the 100 kA arc should have a the parabolic shape of Eq. 1 with $D = [IB/(2mv_z^2)] = [(100\text{ kA}) \cdot (50 \times 10^{-4}\text{ T})] / [2 \cdot (1 \times 10^{-4}\text{ kg/m}) \cdot (10^3\text{ m/sec})^2] \approx 1\text{ m}^{-1}$ Thus if the arc has a vertical height of 1 m, it should have a horizontal deflection of about 1 m at the anode, i.e., its deflection angle should be ≈45^o. This appears to be similar to angles believed to occur in some large furnaces.

For other DC arc furnaces, the arc deflection coefficient D can be estimated from the following approximate scalings: $B \propto I/R$ from simple magnetics, $m \propto I^{1/2}$ for arcs at fixed current density and temperature at atmospheric pressure, and $v_z \propto I^{1/2}$ from Eq. 2 for a fixed current density at the cathode spot, implying $D \propto I^{1/2}/R$. Thus the arc deflection at the anode due to the magnetic fields from external buswork would tend to largest in furnaces with high current where the buswork was close to the arc, and would increase as the square of the arc length, according to the model of Eq. 1.

b) Effect of magnetic materials on arc deflection:

A permeable iron shell in an industrial-scale DC furnace could significantly reduce the magnetic field due the buswork at the location of the arc. The magnetic shielding effect of permeable iron can be roughly estimated using a simple 1-dimensional model, assuming complete saturation of the iron at B = 10 kG. The thickness of iron needed to shield the magnetic flux from a field of 50 Gauss extending over a length of 5 m from the buswork would be $\approx$(50 G/10,000 G)$\cdot$ 5 m $\approx$ 2.5 cm. This is similar to the thickness of large furnace shells, so the existing iron shells should have a significant influence on the estimate of arc deflection given in Sec. 5(a). The magnetic field at the arc would be a complicated function of buswork routing and the leakage of magnetic field through the various holes in the shell.

The scrap iron and steel inside the furnace will most likely shield the magnetic field of the buswork from the arc during the initial meltdown, but only when the temperature of the scrap was below the Curie temperature ($\approx$700^o C), above which it becomes non-magnetic. Below this temperature the magnetization of the scrap by the currents inside the furnace would probably dominate the arc behavior and cause random deflections of the arc, but these deflections would probably not reach or damage the refractory wall.

c) Possible methods to control DC arc deflection

The simplest way to control arc deflection would be to apply a horizontal magnetic field similar to the experiments described in Sec. 3. Two pairs of magnetic coils 90^o apart outside the furnace shell could null out arc deflection in any direction, assuming the effect of the iron shell was taken into account properly. Current for these coils can be tapped from the arc power supply, and their power consumption should be comparable to the rest of the buswork. A second strategy would be to thicken the soft iron shell to ensure

that any stray magnetic field caused by the buswork did not penetrate into the furnace.

A third strategy would be to somehow increase the arc mass density or arc jet speed, since both enter into the deflection coefficient D in Eq. 1. For a given arc current, the arc jet speed might be increased by reducing the radius of the cathode spot, which could possibly be done by increasing the current density emitted at the cathode surface using a different cathode composition. The arc density might be increased by reducing the arc temperature, e.g., by introducing more cold gas near the cathode spot. The effect of the foamy slag around the arc might also be considered as an indirect means to increase in the effective mass density of the arc.

d) Arc deflection in AC furnaces

As an aside, we note that the arc deflection formula Eq. 3 is valid on timescales long compared with the transit time of the arc jet between the cathode and anode, which is ≈1 msec for an EAF arc of length ≈1 m at an estimated arc speed of 1,000 m/sec. Therefore this model should also be valid for arcs in 3-phase AC furnaces [21]. However, the dominant transverse magnetic field for a given arc in that case would be from the other two electrodes, which are much closer to any given arc. Thus the AC arc deflection vs. time could be modeled fairly easily based on analysis similar to that leading to Eq. 1.

e) Cathode spot instability model applied to large DC furnaces

Let us assume that a DC arc furnace of 100 kA has an arc jet speed of $v_z \approx$ 1,000 m/sec, a cathode spot radius of $r_c \approx 3$ cm, and an arc length of $L \approx 1$ m (as in Sec. 5(a). According to the model of Sec. 4, if the cathode spot motion has a radius of $a \approx r_c \approx 3$ cm (i.e. similar to their relationship in our experiment), and if the instability frequency is 100 Hz, then the arc would have a horizontal velocity of $v_y = \omega a \approx 20$ m/sec, and so its position at the anode would move with a radius of $L \cdot (v_y/v_z) \approx 2$ cm. Such a small motion would probably not cause the noise and voltage fluctuations observed in the actual furnaces.

However, in EAFs there is a turbulent spectrum of fluctuations in the range ≈ 10-1000 Hz. At ≈10 Hz the transverse cathode spot velocity would be so slow that the arc would remain perpendicular to the cathode surface, and so its location at the anode would probably be determined by the local curvature of the cathode tip. At 1,000 Hz there would be one axial

wavelength of the arc between the cathode and the anode, and the horizontal cathode spot speed would be ≈200 m/sec, corresponding to displacement at the anode of ≈20 cm.

It is likely the actual motion of the arc during instability is larger than these estimates, so either the cathode spot movement is larger than assumed above, or there is some other physical mechanism driving arc instability in large furnaces. Cathode spot speeds of up to ≈100 m/sec and helical (or conical) arc motion have been observed in high current arcs [1,6,16].

f) Control of arc instability in large furnaces

If movements of the cathode spot are the main cause of arc instability, as implied by our experiments, then changes in the cathode temperature distribution, cathode shape, or chemical composition could potentially control this instability. Usually large EAFs use ≈1 m diameter solid graphite cathodes which have a cylindrical shape and a hemispherical tip at the arc end.

The most direct means for arc stabilization in our experiment was to increase the diameter of the cathode. However, EAFs at I = 100 kA are unstable even though the cathode diameter is at least 10 times the cathode spot diameter, in contrast to our experiment where a 250 A arc was stabilized for a cathode diameter of a few times the cathode spot diameter. The stabilization in our experiment was attributed to conductive cooling of the surface adjacent to the cathode spot; however, in the industrial furnace the whole cathode tip may be near 3,500 ^{o}C due to its immersion inside the furnace. If so, one route to arc stabilization might be to reduce the temperature of the cathode tip, perhaps by moving it nearer to the top of the furnace shell.

Stabilization in our experiment was also seen when the cathode radius was very small, i.e., comparable to the cathode spot radius. Thus another route to arc stabilization in large EAFs might be to reduce the locally effective tip diameter to the size of the cathode spot (≈6 cm), thus inhibiting the cathode spot motion and arc instability. Another approach to arc stabilization would be to minimize the cause of the cathode spot movement. If this motion is caused by graphite evaporation at the cathode spot, as described in Sec. 4(e), then the arc instability might be controlled by reducing the evaporation rate of the cathode. This would also increase the lifetime of the cathode, but may be difficult or costly in practice.

Finally, adding an axial magnetic field to an arc could potentially increase its stability, analogously to the stabilization of fusion plasmas. Such a method was proposed and tested on a small-scale experiment [17]. In our case, a weak vertical magnetic field created a new high frequency instability, and a strong vertical magnetic field extinguished the arc [5]. However, such fields have been used in industrial furnaces for stirring the liquid metal bath, and may allow some degree of control over arc instability.

6. Needs for Further Research

Of course, conclusions from these small-scale experiments should not be directly applied to the design of large-scale EAFs without further research, since large industrial arcs have some different physical parameters and a different environment than the small arcs in our experiment. Although some good research has already been done on high-current arcs [1,2], relatively little is known about the behavior of arcs inside large EAFs, due to their inaccessibility and complexity.

The main parameter differences between our experiment and an industrial arc are summarized in Table 1. The arc jet speed is likely to be ≈10-100 times higher in industrial furnaces. The Mach number of the arc jet may be ≥1, which could cause shock waves and significantly modify the arc stability. The hydrodynamic Reynolds number of the industrial arc jet will probably be in the range of $R_H \approx 1{,}000$, making strong turbulence much more likely. In general, the behavior of plasmas with supersonic flow and strong turbulence is not well understood, and so this would be an interesting a subject for future research.

The industrial arc furnace environment is also considerably more complicated than our experiment, since it contains foamy slag around the arc, unmelted metal scrap and/or splashing liquid metal, convective flows of gases and metal, and uncertain current distributions inside the cathode and liquid metal anode. Each of these factors (and probably many others) can affect arc deflection and instability in the real furnace, and none of them is accounted for in our model. Therefore research is needed to identify and model these effects on arc behavior in industrial furnaces.

Another possible difference between the physics of low and high current arcs is the degree to which self-generated magnetic fields can affect the arc behavior, as reflected in the plasma β (ratio of plasma pressure to magnetic pressure) and the magnetic Reynold's number R_M in Table 1. Large self-magnetic fields generally cause plasma instability, although their effect was probably negligible in our experiment [5]. It is likely that high current

furnace arcs have some magnetically self-generated instability, as discussed in the literature [1,16,18].

These small-scale arc experiments at PPPL are completed, but our laboratory would be interested in partnering with industry to continue this research on larger-scale furnaces. Progress in such research would depend on the application of state-of-the-art diagnostic and computational tools for measuring and simulating the complicated behavior of the arc plasma, neutral gas, and molten metal inside these furnaces.

7. Summary and Conclusions

A set of experiments and modeling was done to understand the arc deflection and instability observed in a I = 250 A DC arc where the graphite cathode and steel anode were meant to simulate the behavior of an industrial-scale EAF. The arc deflection due to an external magnetic field B was explained by a simple model of the I × B force on the arc jet. The instability observed in this experiment was explained by the unstable movement of the arc attachment spot at the cathode, rather than by an instability of the arc itself. Some potential applications of these results to industrial-scale furnaces were described, but clearly more research is needed before the arc deflection and instability of high-current furnaces can be understood and directly controlled.

Acknowledgments: We thank H.P. Furth, R.C. Davidson, and R.J. Goldston of PPPL for supporting this work, which was done under US Department of Energy Contract #DE-AC02-76-CH03073. We also thank for their technical assistance A. Brooks, P. Heitzenroder, L. Roquemore, and L. Zakharov of PPPL, and for helpful discussions P. M. Bellan, G. Bendzsak, B. Bowman, J. Heberlein, and S.-E. Stenkvist. Finally, we thank the representatives of ABB and the operators of Charter Steel for allowing us to visit their furnace.

References:

1) Ben Bowman, "Properties of Arcs in DC Furnaces," EAF Conference Proceedings Vol. 52, Nashville (1994) p. 111.

2) G.R. Jones, High Pressure Arcs in Industrial Devices: Diagnostic and Monitoring Techniques, Cambridge University Press, Cambridge 1988.

3) E. Pfender, "Electric Arcs and Arc Gas Heaters" in Gaseous Electronics, Vol. 1: Electrical Discharges, Chapter 5, Academic Press, NY 1978.

4) R.J. Hawryluk, Rev. Modern Physics Vol. 70, 537, 1998.

5) M. Karasik, "Driven Motion and Instability of an Atmospheric Pressure Arc," Ph.D. Thesis, Princeton University (January 2000), available as PPPL Report #3398 (1999) at http://www.pppl.gov/pub_report.

6) N. Ao and M. Nakai, "Prevention of arc deflection and electro-magnetic stirring in DC Arc furnaces," SEAISI Quarterly, p. 20, 1994.

7) G. Speckhofer and H.P. Schmidt, "Experimental and theoretical investigation of high-pressure arcs - part II: The magnetically deflected arc (three dimensional modeling)," IEEE Trans. Plasma Sci. 24(4), 1239, 1996.

8) G.J. Bendzsak and E.G. Mueller, "Steel Bath circulation and arc deflection in DC furnaces," Modern Steelmaking and Casting Techniques, p. 137.

9) M. Karasik, A.L. Roquemore, and S.J. Zweben, "Experiments and Modeling of an Atmospheric Pressure Arc in Applied Oscillating Magnetic Field," accepted for publication in Physics of Plasmas (2000).

10) J.F. Lancaster, ed. The Physics of Welding, Pergamon Press, 2nd Edition, 1986.

11) H. Maecker, "Plasma Streaming in Arcs due to Self-Magnetic Compression," Z. fur Physik 141, 198, 1955; also, "Principles of arc motion and displacement," Proc. IEEE 59(4), 439, 1971.

12) Y. Raiser, Gas Discharge Physics, Springer-Verlag, New York, 1991.

13) D.H. McQueen, Noise From Electric arc furnaces I: General Considerations", Scandinavian Journal of Metallurgy 7, 5, 1978.

14) S.-E. Stenkvist, "Single Electrode DC arc Furnace," Iron and Steel Engineer 62, 50, 1985; also, S.-E. Stenkvist and B. Bowman, "High-Power, Graphite Cathode DC Arc Plasma - Properties and Practical Applications for Steelmaking and Ferroalloys Processing," Ch. 8B, Plasma Technology in Metallurgical Procession, p. 103, Jerome Feinman, Ed., Published by the Iron and Steel Society, 1987.

15) B. Bowman, G.R. Jordan, and F. Fitzgerald, "The Physics of High Current Arcs," J. of Iron and Steel Society, p. 798, 1969.

16) G.R. Jordan, B. Bowman, and D. Wakelam, "Electric and photographic measurements of high powered arcs," J. Phys. D: Applied Phys. 3:1089 (1970).

17) P.M. Bellan and J. W. Higley, IEEE Trans. Plasma Sci. 20, 1026, 1992.

18) K. Ragaller, Z. Naturforsch 29a, 556, 1974.

19) P.E. King, T.L. Ochs, and A.D. Hartman, J. Appl. Phys. 76, 2059, 1994.

20) M. Karasik and S.J. Zweben, "Experiments and Modeling of an Instability of an Atmospheric Pressure Arc," submitted to Phys. Plasmas (2000).

21) H.L. Larsen, G. Saevarsdottir and J.A. Bakken, "Simulation of AC arcs in the Silicon Metal Furnace," Electric Furnace Proc. 54, 157, 1996.

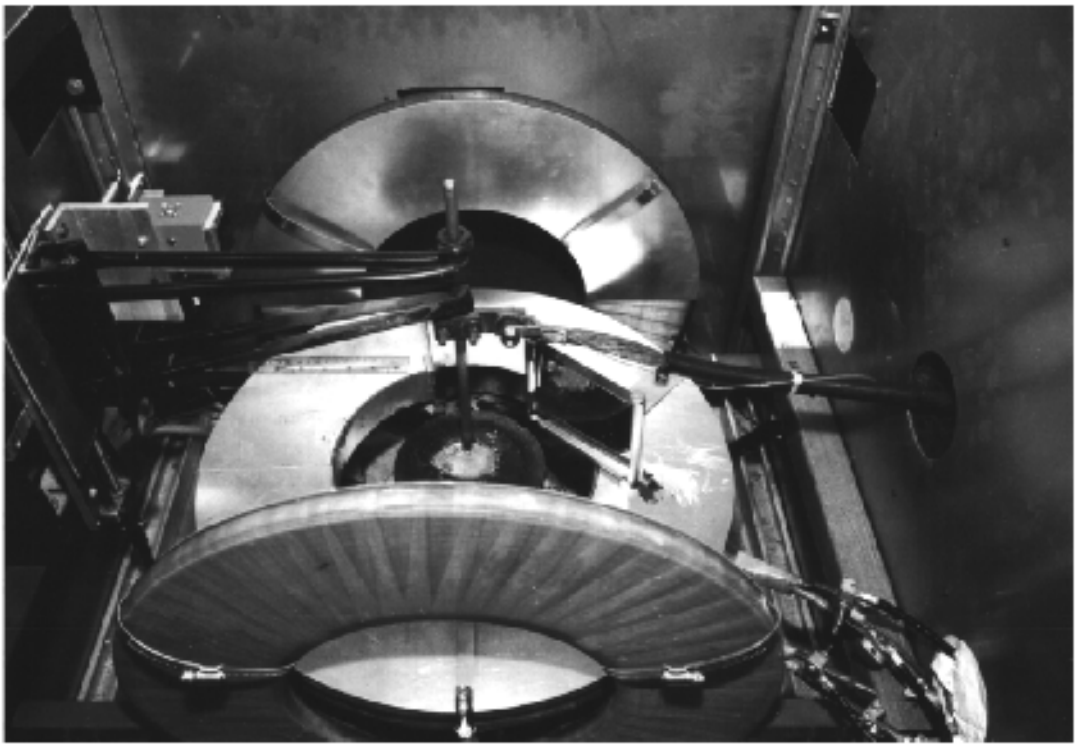

Fig. 1: Photograph of the PPPL arc furnace. The steel furnace anode in the center has a diameter of 6", and the graphite cathode shown just above it has a diameter of typically 3/8". The transverse magnetic field coils are shown in the foreground and behind the furnace, and the vertical magnetic field coils are below the furnace. The current feeds enter from the right side, and the cathode position control is at the left. The 90° mirror is just to the right of the anode.

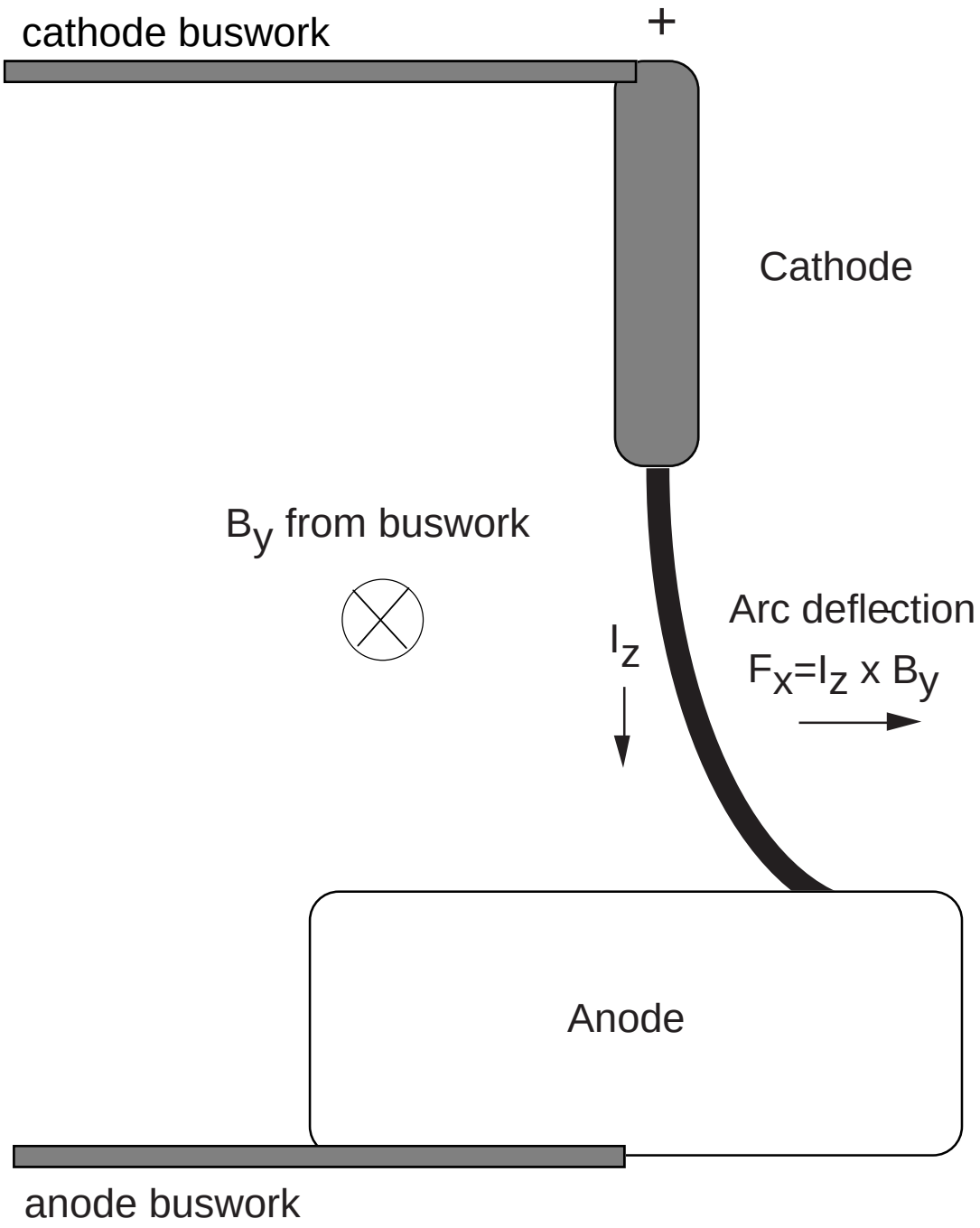

Fig 2: Schematic diagram of arc defelction in a DC furnace. The arc current I_z is acted upon by a force $F_x = I_z \times B_y$ due to the magnetic field created by the buswork B_y. This causes the arc to be deflected away from the power supply. This model ignores the effect of magnetic material around the furnace, which may be important in practise.

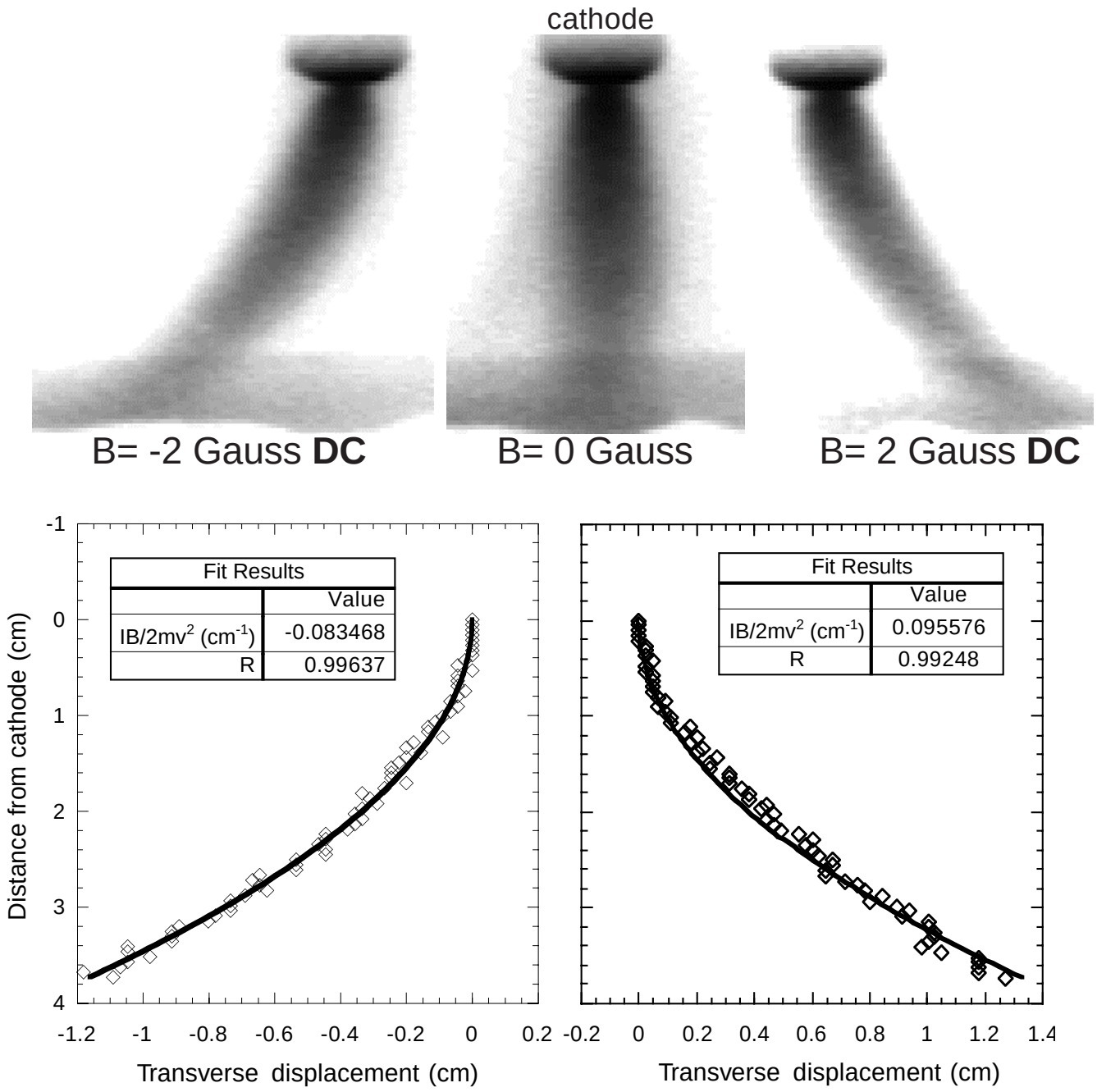

Fig. 3: Arc deflection due externally applied DC magnetic fields. The photos at the top are negatives of CCD images of the arc deflection for two different transverse DC magnetic fields (±2 Gauss). The arc is about 4 cm in length and connects the graphite cathode with the molten steel anode. These pictures were taken with a 10 μsec exposure time and compressed vertically by 2.4:1. At the bottom are fits between the digitized shape of these arcs and the model of Eq. 1. These arcs fit the parabolic shape of Eq. 1 and were used to determine the arc deflection coefficient $D=[IB/2mv^2]$.

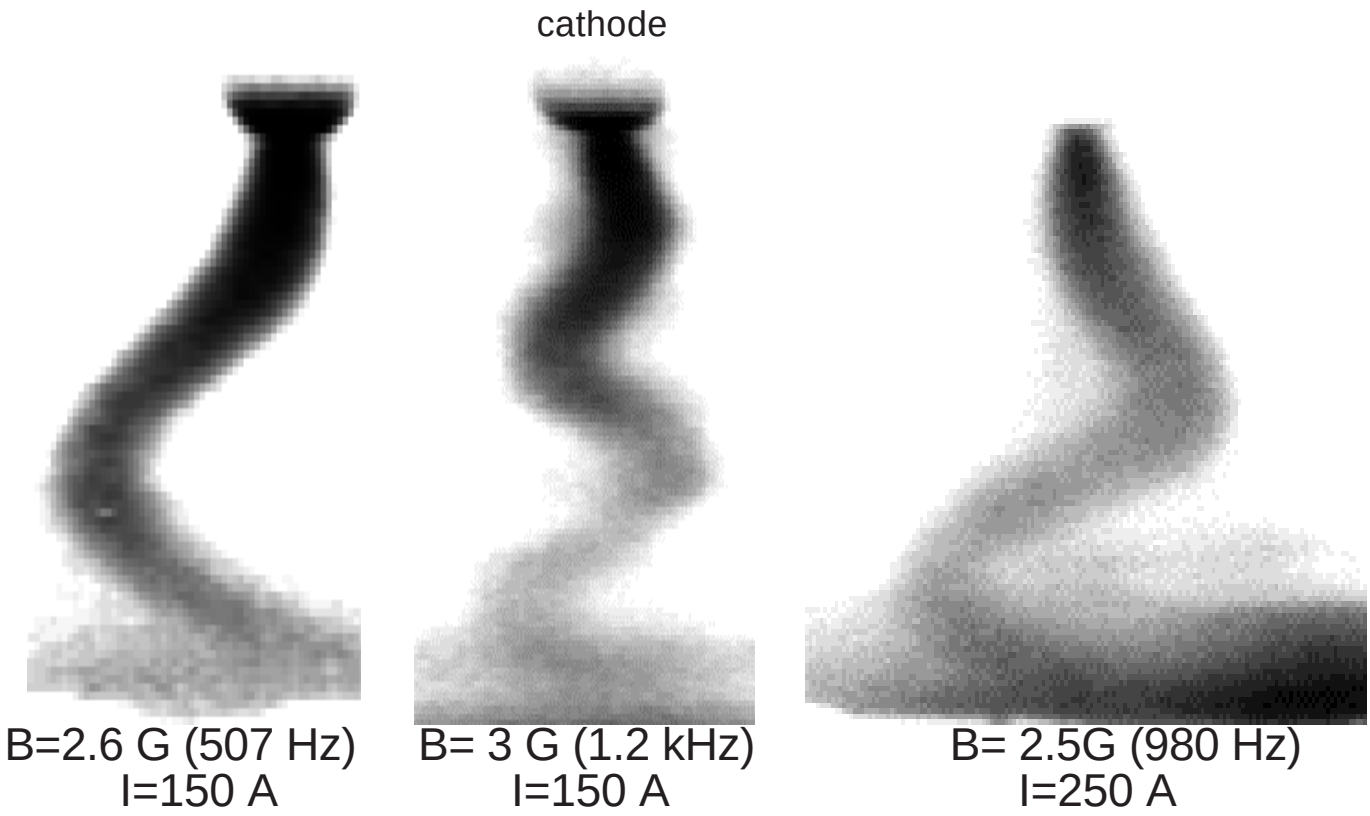

Fig. 4: Sample images of the externally driven oscillatory motion of the arc at different frequencies and applied AC magnetic fields. The geometry and camera set-up is the same as figure 3. The axial wavelength is shorter for higher applied frequencies, as shown by the comparison between the left and middle images, and the wavelenght increases with increasing current, as shown by the comparison between the middle and right images. At each vertical position the arc oscillates horizontally in time at the applied frequency.

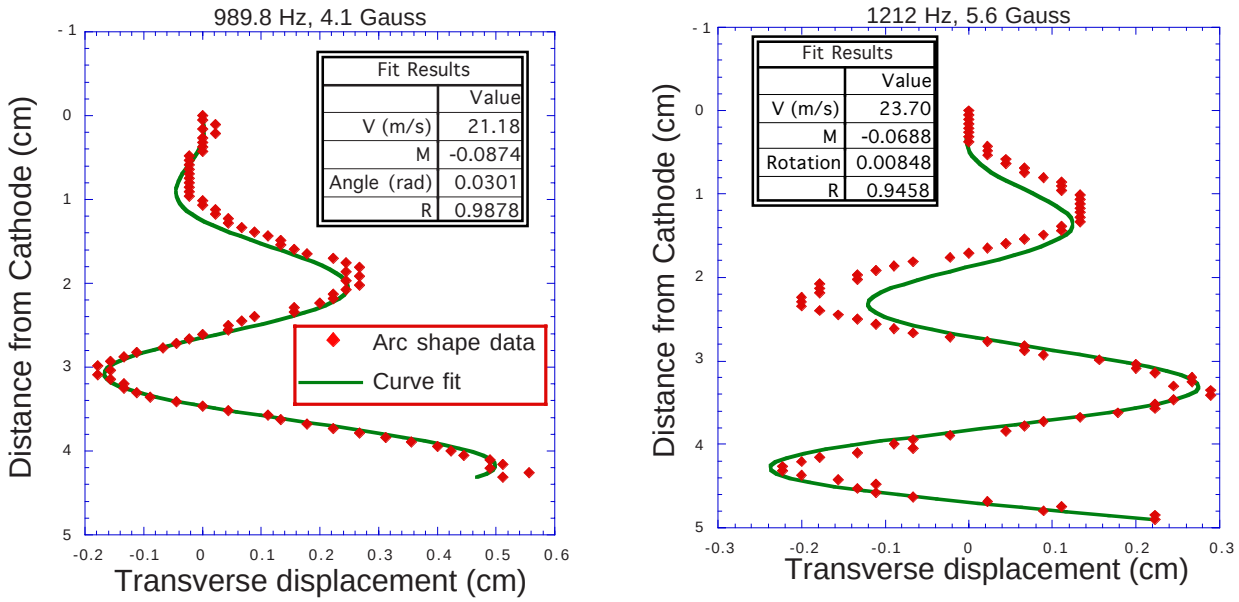

Fig. 5: Examples of experimentally-obtained arc shapes fit by the AC arc deflection model of Eq. 3. From these fits can both the arc speed and linear mass density can be inferred. The horizontal scales are enlarged as shown, and the arc current is 150 A. in both cases.

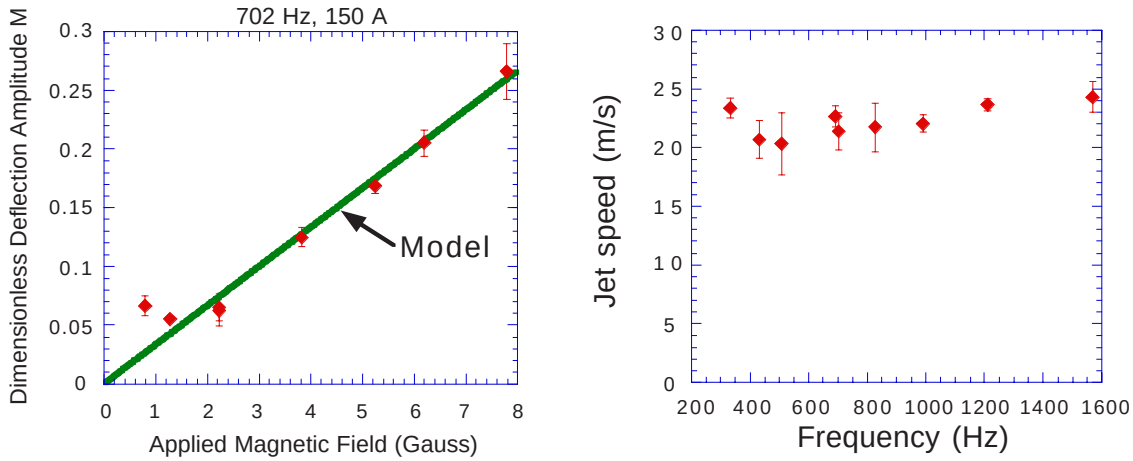

Fig. 6: On the left is the relationship between the externally applied AC magnetic field and the magnitude of the arc deflection coefficient inferred from a fit of the arc shapes to the model of Eq. 3. The good fit with the model implies that the arc deflections increase linearly with the applied field, as expected. On the right is the arc jet speed inferred from fits to the same model as a function of the applied AC frequency. The inferred speed is about the same at all frequencies, as expected, since the speed is determined by the arc jet.

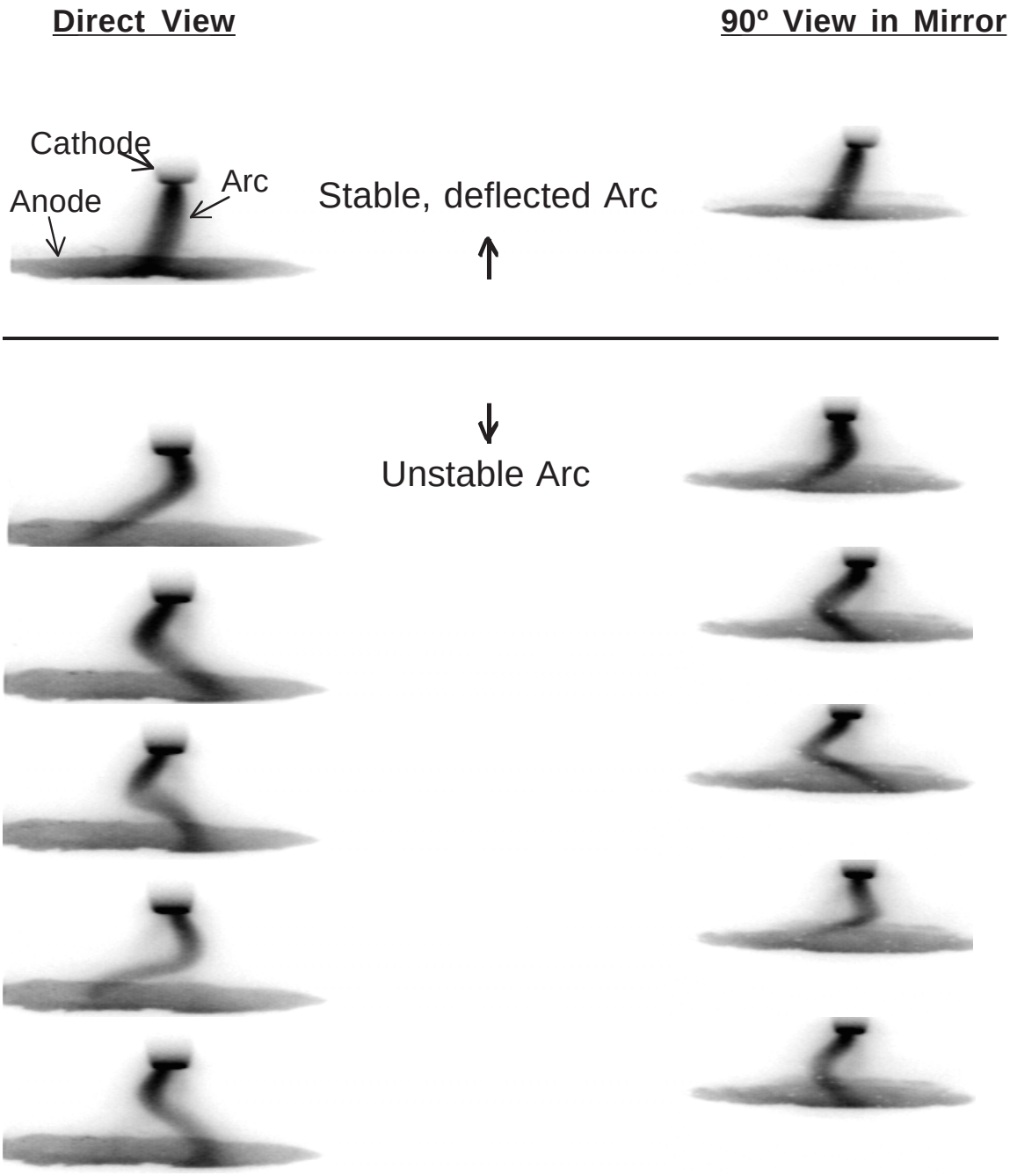

Fig. 7: Sample images of an unstable arc during low amplitude oscillations. The left-hand column shows a direct view of the arc from the CCD camera, while the right-hand side shows the same arc in the 90° mirror. The five unstable frames were picked from a 30 frame data set to illustrate the different arc column shapes. These images were each exposed for 10 μsec, and the cathode-anode gap is 3.1 cm. The horizontal scales are expanded by a factor of 2.4:1 on the left and 2.3:1 on the right.

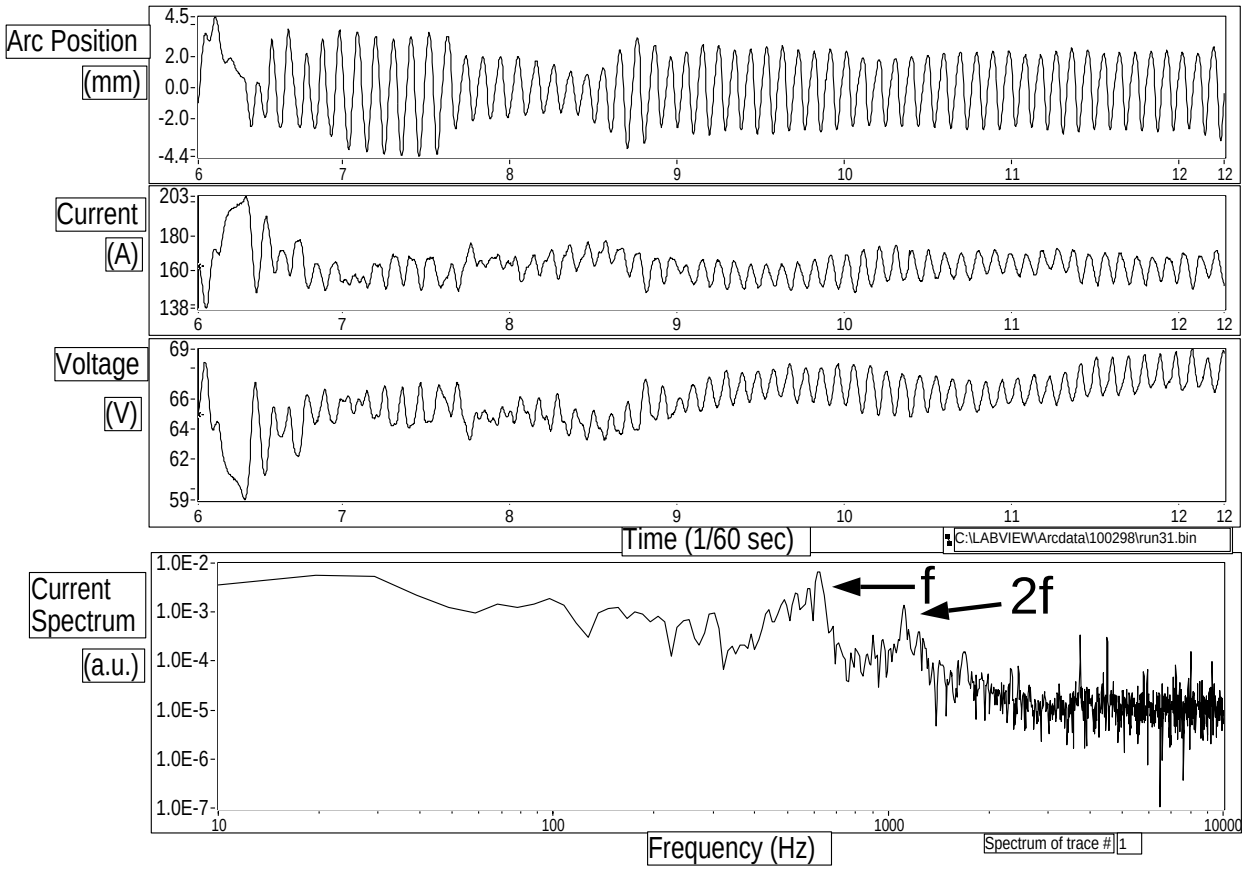

Fig. 8: Time dependence of arc parameters during a low-amplitude 600 Hz arc instability. The timescale is marked in units of 1/60th second, corresponding to CCD camera frames taken at the same time. The arc position is determined from a horizontal linear array of photodiodes viewing the arc at a fixed distance above the anode. Both the arc current and voltage show few-% fluctuations at the fundamental frequency of 600 Hz. The frequency specturm of the current and voltage also show power at the second harmonic, as shown at the bottom.

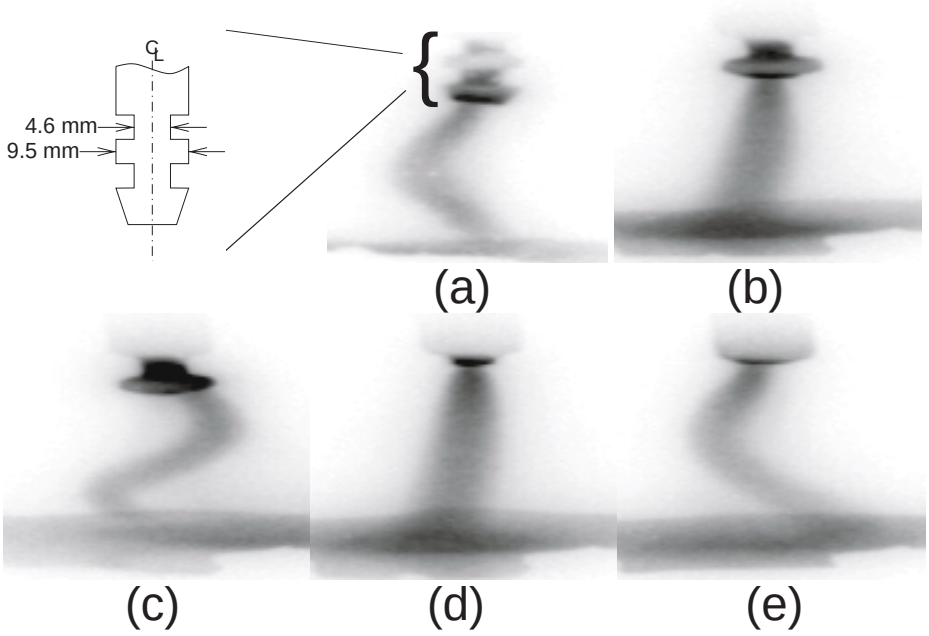

Fig. 9: Photographs of the arc behavior with a "necked" cathode, in which the cathode diameter varies along the length of the cathode, as illustrated at the top left. During a single run at I = 250 A with this cathode, the arc was unstable when the cathode diameter was 9.5 mm, as shown in the photos in (a), (c), and (e), but was stable when the cathode wsa 4.6 mm diameter, as shown in the photos in (b) and (d). This demonstrated the effect of cathode size on arc instability in this experiment. The horizontal scale is expanded 2.4:1 in all photos.

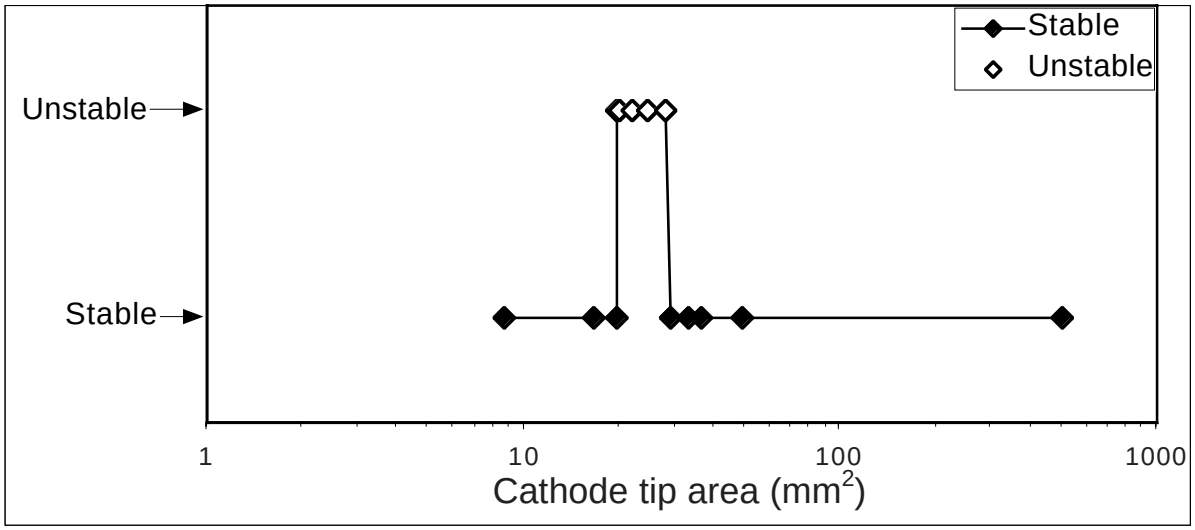

Fig. 10: Effect of the cathode size on the stability of arcs in this experiment. For cylindrical cathodes the arc at I = 25 A is unstable only for cathode areas of 20-30 mm^2. This illustrates the effect of cathode geometry on arc stability.

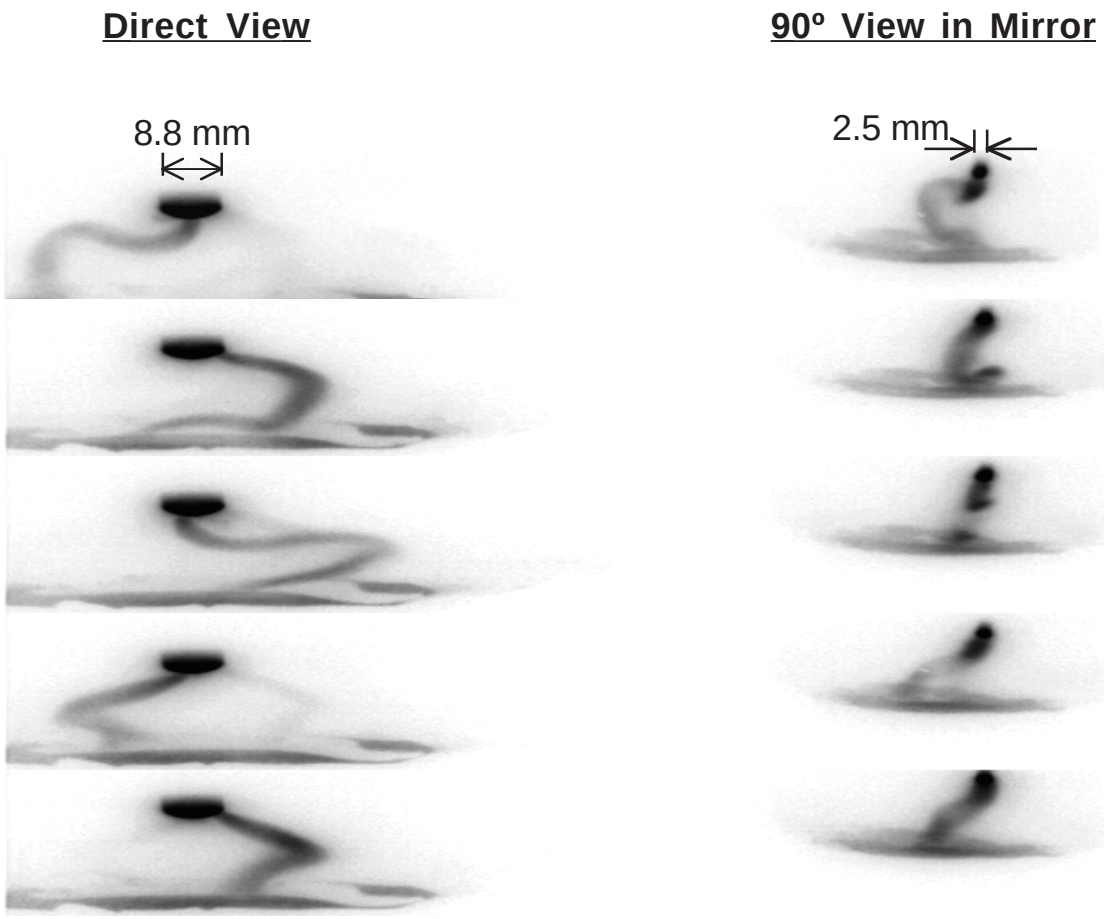

Fig. 11: Sample pictures of an unstable arc during a large amplitude oscillation with a "paddle" shaped cathode, which was 8.8 mm wide by 2.5 mm thick. The left-hand column shows a direct view of the arc, and the right-hand side shows the same arc in the 90° mirror. These images were each exposed for 10 μsec, and the cathode-anode gap is 2.7 cm. The horizontal scales are expanded by a factor of 2.4:1 on the left and 2.3:1 on the right. Note that the cathode is wider in the direct view plane and that the amplitude of arc motion is larger in this plane. Also note that the arc attachment is moving along the tip of the cathode.

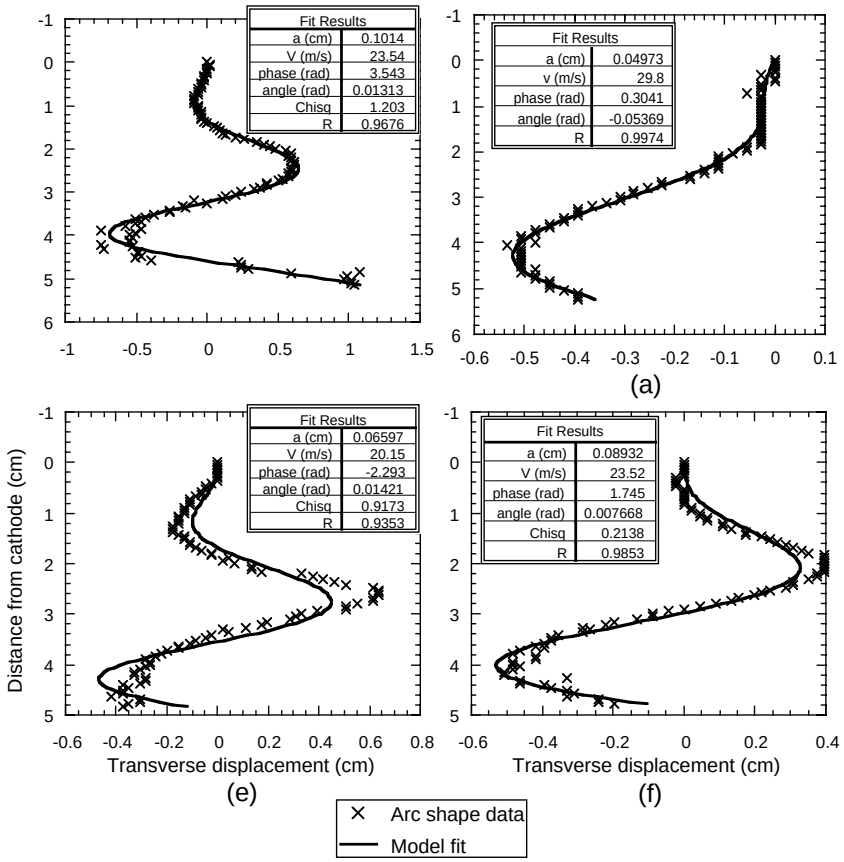

Fig. 12: Examples of experimentally-obtained unstable arc shapes fit to the model of Eq. 4. The "x" points are the data from arc shapes taken from digitized CCD images, and the smooth lines are solutions of the model equation. The four cases shown have arc currents and frequencies of (a) 250 A, 575 Hz, (b) 220 A, 780 Hz, (c) 197 A, 650 Hz, and (d) 222 A, 600 Hz. Note that the horizontal scales vary from case-to-case.

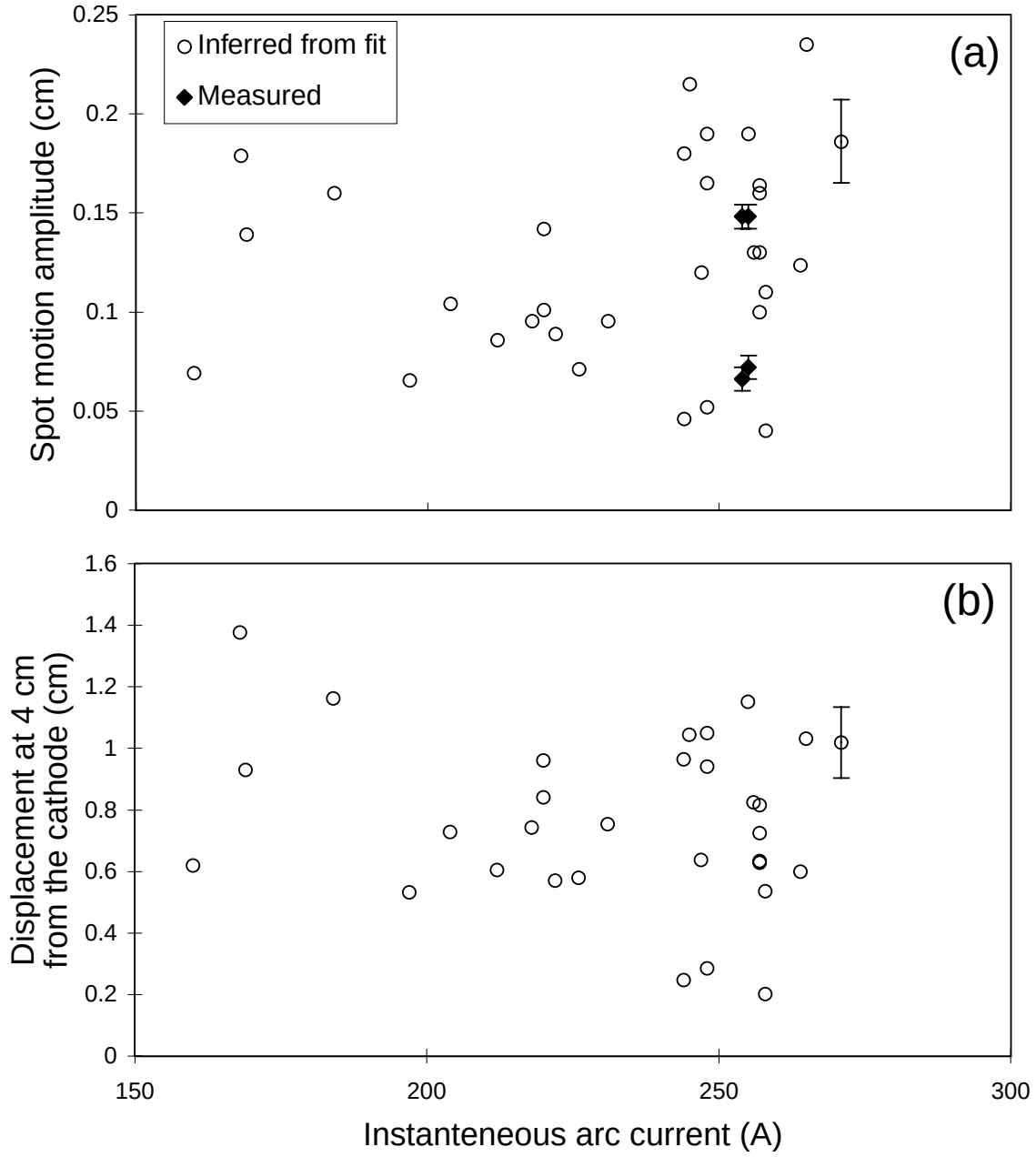

Fig. 13: At the top are cathode the spot motion amplitudes for unstable arcs vs. arc current. The amplitudes inferred from fits of the model to the observed arc shapes (open circles) are consistent with direct measurements of the cathode spot motion (closed diamonds). At the bottom are the maximum arc displacements measured 4 cm axially from the cathode for the same data set as the top. There is no apparent trend of arc displacement vs. current in this range of data.

Parameter	Definition	Magnitude	
		PPPL Arc	Industrial Arc
Power (peak)	VI	25 kW	100 MW
Temperature	$T_e = T_i = T_n$	1 eV	1-2 eV
E-field (arc column)	E	10 V/cm	10 V/cm
Current (peak)	I	250 A	100 kA
Self B-field	$B_{\rm self}$	200 G	6 kG
Pressure	$p = nkT$	1 atm	$\gtrsim$ 1 atm
e^- Density (peak)	n_e	10^{17} cm^{-3}	$\gtrsim 10^{17}$ cm^{-3}
Characteristic Arc Dia.	L	0.6 cm	10 cm
Cathode Spot Radius	r_c	1.3 mm	2.5 cm
Ionization fraction (%)	n_e/n	$\sim 10\%$	10–100%
Debye Length	$\lambda_D = \sqrt{\frac{kT\epsilon_0}{4\pi n_e^2}}$	10^{-6} cm	10^{-6}
Plasma Parameter	$(4\pi/3)n_e\lambda_D^3$	~ 5	~ 5
Plasma Frequency	$f_{pe} = \sqrt{\frac{n_e e^2}{4\pi^2\epsilon_0 m_e}}$	10^{12} Hz	10^{12} Hz
Ion Gyrofrequency	$f_{ci} = \frac{eB_{\rm self}}{2\pi m_i}$	10^4 Hz	10^5 Hz
Ion Gyroradius	$\rho_{Li} = \frac{\sqrt{kT/m_i}}{2\pi f_c i}$	2 cm	0.6 mm
e^- Collision Frequency	$\nu_e = \frac{n_i e^4 \ln\Lambda/\pi^2\epsilon_0^2}{12\sqrt{2m_e}(kT_e)^{3/2}}$	10^{11} sec^{-1}	10^{11} sec^{-1}
e^- Mean Free Path	$\lambda_{{\rm mfp},e} = \frac{\sqrt{kT/m_e}}{\nu_e}$	10^{-5} cm	10^{-5} cm
Conductivity	$\sigma = (I/\pi L^2)/E$	80 Ω^{-1}cm^{-1}	100 Ω^{-1}cm^{-1}
Resistive Diffusion Time	$\tau_R = \mu_0 L^2\sigma$	10^{-7} sec	10^{-4} sec
Alfvén Speed	$V_A = B_{\rm self}/\sqrt{\mu_0\rho}$	10^4 cm/s	10^5 cm/s
Magnetic Reynolds #	$R_m = \tau_R V_A/L$	10^{-3}	~ 1
Plasma β	$\beta = \frac{p}{(B_{\rm self}^2/2\pi\mu_0)}$	~ 1000	~ 1
Plasma jet speed (peak)	$v_{\rm jet} = I\sqrt{\frac{\mu_0}{2\pi^2 r_c^2\rho}}$	10^4 cm/s	10^5 cm/s
Mach number (peak)	M	10^{-2}	~ 1
Hydrodyn. Reynolds #	$R_H = v_{\rm jet} r_c/\eta$	10	10^3

Table 1: Approximate arc parameters for the PPPL furnace (left) and a 100 MW industrial-scale DC furnace (right).